Homotopy Analysis Method for Limit Cycle Oscillations of an Airfoil with Cubic Nonlinearities

Y.M. Chen and J.K. Liu

Journal of Vibration and Control 2010 16: 163 originally published online 20 October 2009
DOI: 10.1177/1077546308097268

Homotopy Analysis Method for Limit Cycle Oscillations of an Airfoil with Cubic Nonlinearities

Y. M. CHEN
State Key Laboratory of Mechanical System and Vibration, Shanghai Jiao Tong University, 800 Dongchuan Road, Shanghai 200240, China

J. K. LIU
Department of Mechanics, Sun Yat-sen University, Guangzhou 510275, China
(jikeliu@hotmail.com)

(Received 30 January 2008; accepted 9 July 2008)

Abstract: An analytical approximate technique for nonlinear problems, namely the homotopy analysis method, is employed to propose an approach for the aeroelastic system of a two-dimensional airfoil with a cubic nonlinearity. The frequency and amplitude of the limit cycle oscillation are expanded as power series of an embedding parameter. A series of algebraic equations governing the coefficients of the series are then derived. All the equations are linear except the first one. This provides us with a simple iteration scheme to seek high-order approximations. The frequency and amplitude of the limit cycle oscillation are obtained with a high degree of accuracy. It turns out that the frequency is independent of the coefficient of the cubic nonlinearity, and that the amplitude is in inverse proportion to the square root of this coefficient.

Keywords: Homotopy analysis method, airfoil, nonlinear aeroelastic system, limit cycle oscillation.

1. INTRODUCTION

The most widely applied analytical technique for nonlinear problems is probably the perturbation method (Nayfeh, 1981). The underlying idea of the perturbation technique is to transform, by means of small parameters, a nonlinear problem into an infinite number of simpler, usually linear, subproblems. Consequently, the accuracy of perturbation approximation strongly depends on the small parameter. If the perturbation parameter is not small enough, the approximation may even cease to be valid. In principle, the perturbation method works only for problems containing small parameters.

Recent years have witnessed an increase of interest in the application of the homotopy technique (Alexander and Yorke, 1978) in nonlinear problems. Its attraction lies in the fact that the homotopy method continuously transforms a difficult problem into a simpler problem by means of an embedding parameter p. An analytic approach, namely the homotopy analysis method (Liao, 2003), was proposed by introducing an auxiliary parameter λ to construct a kind of homotopy in a rather general form. Its main procedure is to transform the nonlinear problems, by means of the embedding parameter p rather than the small parameter that is used in the perturbation technique, into an infinite set of subproblems. Note that,

Journal of Vibration and Control, **16(2):** 163–179, 2010 DOI: 10.1177/1077546308097268

unlike the perturbation technique, the homotopy analysis method does not require any small or large parameters at all. Additionally, the auxiliary parameter λ provides a convenient way to control the convergence of approximation series and to adjust convergence regions when necessary (Liao, 2003).

For many strongly nonlinear problems, the convergence of homotopy analysis approximations can be guaranteed by the appropriate choice of the auxiliary parameter λ. Liao (2004) showed that, for the van der Pol equation, the approximations can be valid for very large values of the nonlinear coefficient, say larger than 40, as long as the auxiliary parameter is appropriately chosen. For the Duffing equation and oscillating equation with quadratic nonlinearity, the homotopy analysis method can even work for all values of the nonlinearity coefficient (Liao, 2003). More recently, new applications of the homotopy analysis method in strongly nonlinear problems are presented in El-Wakil and Abdou (2008). As shown later in this paper, the homotopy analysis method is also proved to be effective for the aeroelastic system of an airfoil no matter how large the coefficient of the cubic nonlinearity is. By and large, it is just the auxiliary parameter λ that makes the homotopy analysis method a powerful technique for strongly nonlinear problems.

An airfoil aeroelastic system is a typical self-excited system. As the flow velocity increases beyond the linear flutter speed, the airfoil oscillates with a limited amplitude, namely, the limit cycle oscillation. Predicting amplitude and frequency of flutter oscillations via analytical or numerical techniques has been an active area of research for many years. Three main methods – the describing function technique, the center manifold theory and the high-dimensional harmonic balance method – have been widely used in analyzing the limit cycle behavior.

The describing function technique, sometimes referred to as the harmonic balance or linearization method, is used to obtain an equivalent linear system such that traditional linear aeroelastic methods of analysis can then be employed (Lee et al., 1999). Ueda and Dowell (1984) applied this technique to aerodynamic nonlinearities in the analysis of a typical section subject to transonic aerodynamics. Also, this technique was employed by Liu and Zhao (1992), Price et al. (1995), and Shahrzad and Mahzoon (2002) to study a typical airfoil section containing structural nonlinearities.

The aeroelastic model of a two-dimensional airfoil in unsteady flow is inherently infinite-dimensional. Lee et al. (1997) reduced it to a system of eight first-order ordinary differential equations. Employing the reduced system, Liu et al. (2000) used the center manifold theory to predict the fundamental frequency of the limit cycle oscillation. However, because the center manifold theory is essentially a local method, the accuracy of the prediction decreases as the flow velocity increases.

In recent years, the high-dimensional harmonic balance method has widely applied in nonlinear aeroelastic problems. Lee et al. (2005) investigated the nonlinear aeroelastic system by the harmonic balance method with two dominant harmonics. The high-dimensional harmonic balance method was also successfully employed and improved to deal with aeroelastic problems (Liu and Dowell, 2004; Liu et al., 2007). In addition, the incremental harmonic balance method, a semi-analytical method for nonlinear dynamic systems, was used by Raghothama and Narayanan (1999) to address the dynamic behavior of a two-dimensional airfoil with cubic pitching stiffness.

The accuracy of the approximate solutions given by harmonic balance method is somewhat more satisfactory when flow speeds are relatively low. However, the error becomes

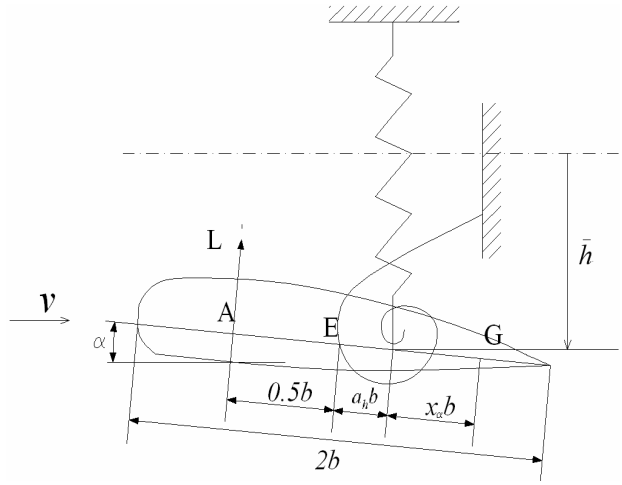

Figure 1. Sketch of a two-dimensional airfoil.

larger and larger as the flow speed increases (Liu and Zhao, 1992; Price et al., 1995; Shahrzad and Mahzoon, 2002). In some nonlinear flutter cases, the harmonic balance method may cease to be valid. Theoretically, the high-dimensional harmonic method and incremental harmonic balance method can provide approximate solutions with any desired accuracy. It is very difficult to put them into practice. Thus, new methods are desired which can simultaneously guarantee high accuracy for high flow speeds and in more flutter cases – for example, both weakly and strongly nonlinear systems.

In this paper, an approach based on the harmonic analysis method is proposed to study the nonlinear aeroelastic system of an airfoil. This approach is easy to apply as it involves a very simple iteration algorithm. It can achieve excellent approximations for both weakly and strongly nonlinear aeroelastic systems.

2. EQUATIONS OF MOTION

The physical model is a two-dimensional airfoil, oscillating in pitch and plunge, which has been employed by many authors. The symbols used in this model are shown in Figure 1. The pitch angle about the elastic axis is denoted by α, positive with the nose up; the plunge deflection is denoted by $\bar{h}$, positive in the downward direction. The elastic axis is located at a distance $a_h b$ from the mid-chord, while the center of mass is located at a distance $x_\alpha b$ from the elastic axis. Both distances are positive when measured toward the trailing edge of the airfoil.

For nonlinear restoring forces with subsonic aerodynamics, the coupled equations for the airfoil in non-dimensional form can be written as follows (Lee et al., 1997):

$$\ddot{\xi} + x_\alpha \ddot{\alpha} + 2\zeta_\xi \frac{\bar{\omega}}{U^*}\dot{\xi} + \left(\frac{\bar{\omega}}{U^*}\right)^2 G(\xi) = -\frac{1}{\pi\mu} C_L(t) + \frac{P(t)b}{mU^2},$$

$$\frac{x_\alpha}{r_\alpha^2}\ddot{\xi} + \ddot{\alpha} + 2\zeta_\alpha \frac{1}{U^*}\dot{\alpha} + \left(\frac{1}{U^*}\right)^2 M(\alpha) = \frac{2}{\pi\,\mu\, r_\alpha^2} C_M(t) + \frac{Q(t)}{mU^2 r_\alpha^2}, \tag{1}$$

where $\xi = \bar{h}/b$ is the non-dimensional displacement, dots denote differentiation with respect to the non-dimensional time t defined as $t = Ut_1/b$, t_1 is real time, U^* is a non-dimensional flow velocity given by $U^* = U/b\omega_\alpha$, and $\bar{\omega}$ is given by $\bar{\omega} = \omega_\xi/\omega_\alpha$, where ω_ξ and ω_α are the natural frequencies of the uncoupled plunging and pitching modes, respectively. ζ_ξ and ζ_α are the damping ratios, and r_α is the radius of gyration about the elastic axis. $G(\xi)$ and $M(\alpha)$ are the nonlinear plunge and pitch stiffness terms, respectively. $P(t)$ and $Q(t)$ are the externally applied force and moment, m is the airfoil mass per unit length and μ is the airfoil–air mass ratio. $C_L(t)$ and $C_M(t)$ are the lift and pitching moment coefficients, respectively. For an incompressible flow, the expressions for $C_L(t)$ and $C_M(t)$ are given by

$$\begin{aligned}
C_L(t) &= \pi(\ddot{\xi} - a_h\ddot{\alpha} + \dot{\alpha}) + 2\pi\left\{\alpha(0) + \dot{\xi}(0) + \left(\frac{1}{2} - a_h\right)\dot{\alpha}(0)\right\}\varphi(\tau) \\
&+ 2\pi\int_0^t \varphi(t-\sigma)\left\{\dot{\alpha}(\sigma) + \ddot{\xi}(\sigma) + \left(\frac{1}{2} - a_h\right)\ddot{\alpha}(\sigma)\right\}d\sigma, \\
C_M(t) &= \pi\left(\frac{1}{2} + a_h\right)\left\{\alpha(0) + \dot{\xi}(0) + \left(\frac{1}{2} - a_h\right)\dot{\alpha}(0)\right\}\varphi(\tau) \\
&+ \pi\left(\frac{1}{2} + a_h\right)\int_0^t \varphi(t-\sigma)\left\{\dot{\alpha}(\sigma) + \ddot{\xi}(\sigma) + \left(\frac{1}{2} - a_h\right)\ddot{\alpha}(\sigma)\right\}d\sigma \\
&+ \frac{\pi}{2}a_h(\ddot{\xi} - a_h\ddot{\alpha}) - \left(\frac{1}{2} - a_h\right)\frac{\pi}{2}\dot{\alpha} - \frac{\pi}{16}\ddot{\alpha},
\end{aligned} \tag{2}$$

where the Wagner function $\phi(t)$ is given by Jones's approximation (Jones 1940), $\phi(t) = 1 - \psi_1 e^{-\varepsilon_1 t} - \psi_2 e^{-\varepsilon_2 t}$, with the constants $\psi_1 = 0.165$, $\psi_2 = 0.335$, $\varepsilon_1 = 0.0455$, and $\varepsilon_2 = 0.3$.

In order to eliminate the integral terms in equation 2, Lee et al. (1997) introduced four new variables:

$$\begin{aligned}
w_1 &= \int_0^t e^{-\varepsilon_1(t-\sigma)}\alpha(\sigma)d\sigma, \quad w_2 = \int_0^t e^{-\varepsilon_2(t-\sigma)}\alpha(\sigma)d\sigma, \\
w_3 &= \int_0^t e^{-\varepsilon_1(t-\sigma)}\xi(\sigma)d\sigma, \quad w_4 = \int_0^t e^{-\varepsilon_2(t-\sigma)}\xi(\sigma)d\sigma.
\end{aligned}$$

Equations 1 can then be rewritten in a general form containing only differential operators as

$$\begin{aligned}
&c_0\ddot{\xi} + c_1\ddot{\alpha} + c_2\dot{\xi} + c_3\dot{\alpha} + c_4\xi + c_5\alpha + c_6 w_1 \\
+ \;& c_7 w_2 + c_8 w_3 + c_9 w_4 + c_{10}G(\xi) = f(t),
\end{aligned}$$

$$d_0\ddot{\xi} + d_1\ddot{\alpha} + d_2\dot{\xi} + d_3\dot{\alpha} + d_4\xi + d_5\alpha + d_6 w_1$$
$$+ \quad d_7 w_2 + d_8 w_3 + d_9 w_4 + d_{10} M(\alpha) \;=\; g(t). \tag{3}$$

The coefficients $c_0, c_1, \ldots, c_{10}$ and $d_0, d_1, \ldots, d_{10}$ are given in the Appendix. $f(t)$ and $g(t)$ are functions depending on initial conditions, Wagner's function, and the forcing terms:

$$f(t) \;=\; \frac{2}{\mu}\left\{\left(\frac{1}{2} - a_h\right)\alpha(0) + \xi(0)\right\}\left(\psi_1\varepsilon_1 e^{-\varepsilon_1 t} + \psi_2\varepsilon_2 e^{-\varepsilon_2 t}\right) + \frac{P(t)b}{mU^2},$$

$$g(t) \;=\; -\frac{1 + 2a_h}{2r_\alpha^2} f(t) + \frac{Q(t)}{mU^2 r_\alpha^2}.$$

By introducing a variable vector $\mathbf{X} = (x_1, x_2, \ldots, x_8)^T$ with $x_1 = \alpha$, $x_2 = \dot{\alpha}$, $x_3 = \xi$, $x_4 = \dot{\xi}$, $x_5 = w_1$, $x_6 = w_2$, $x_7 = w_3$, and $x_8 = w_4$, equations 3 can then be rewritten as a set of eight first-order ordinary differential equations,

$$\dot{\mathbf{X}} = \mathbf{Y}(\mathbf{X}, t). \tag{4}$$

This equation allows existing methods suitable for the study of ordinary differential equations to be used in the analysis. For more details on equation 4, see Lee et al. (1997) or Liu and Dowell (2004).

For a cubic spring, $M(\alpha)$ is described as

$$M(\alpha) = \alpha + \eta\,\alpha^3, \tag{5}$$

where η is a constant. A similar expression for $G(\xi)$ can be written by replacing α with ξ,

$$G(\xi) = \xi + \gamma\;\xi^3, \tag{6}$$

where γ is a constant.

3. MATHEMATICAL FORMULATION

3.1. Rule of solution expression and initial guess

In this study, we assume that there is no external forcing, that is, $Q(t) = P(t) = 0$ in equation 1. For large values of t when transients are damped out and steady solutions are obtained, we can let $f(t) = g(t) = 0$. Then equation 3 can be rewritten in vector form as

$$\mathbf{M}\ddot{\mathbf{x}} + \boldsymbol{\mu}\dot{\mathbf{x}} + \mathbf{K}\mathbf{x} + \mathbf{C}\mathbf{W}(\mathbf{x}) + \mathbf{F}(\mathbf{x}) = 0, \tag{7}$$

where

$$\mathbf{x} = [\xi, \alpha]^T, \quad \mathbf{W}(\mathbf{x}) = \begin{bmatrix} w_1 & w_2 & w_3 & w_4 \end{bmatrix}^T, \quad \mathbf{F}(\mathbf{x}) = \begin{bmatrix} c_{10}\gamma\,\xi & d_{10}\eta\,\alpha \end{bmatrix}^T,$$

$$\mathbf{M} = \begin{bmatrix} c_0 & c_1 \\ d_0 & d_1 \end{bmatrix}, \quad \boldsymbol{\mu} = \begin{bmatrix} c_2 & c_3 \\ d_2 & d_3 \end{bmatrix}, \quad \mathbf{K} = \begin{bmatrix} c_4 + c_{10} & c_5 \\ d_4 & d_5 + d_{10} \end{bmatrix},$$

$$\mathbf{C} = \begin{bmatrix} c_6 & c_7 & c_8 & c_9 \\ d_6 & d_7 & d_8 & d_9 \end{bmatrix},$$

and the superscript T denotes the transpose.

Under the transformation

$$\tau = \omega\, t, \tag{8}$$

where ω is the priori unknown frequency of the limit cycle oscillation, equation 7 becomes

$$\omega^2 \mathbf{M}\mathbf{x}'' + \omega\, \boldsymbol{\mu}\mathbf{x}' + \mathbf{K}\mathbf{x} + \mathbf{C}\mathbf{W}(\mathbf{x}, \omega) + \mathbf{F}(\mathbf{x}) = 0, \tag{9}$$

where priming denotes differentiation with respect to τ. Using the usual procedure in Liao (2003, 2004), equation 9 is first transformed by $\mathbf{x} = \boldsymbol{\Lambda}\mathbf{y}$, where $\boldsymbol{\Lambda}$ is diagonalized by the amplitudes of limit cycle oscillation of plunge and pitch motions. In this paper, however, we do not use such transformation. It will be proved that this alteration can subsequently lead to significant reductions in computational effort. Since the limit cycle oscillation is independent of initial conditions, we consider such initial conditions as

$$\mathbf{x}(0) = \begin{bmatrix} h & a \end{bmatrix}^T, \quad \mathbf{x}'(0) = \begin{bmatrix} \beta & 0 \end{bmatrix}^T. \tag{10}$$

The limit cycle oscillation of system 9 is periodic motion with the frequency ω, thus $\mathbf{x}$ can be expanded as a Fourier series

$$\mathbf{x} = \sum_{k=0}^{\infty} (\mathbf{c}_k \cos k\tau + \mathbf{s}_k \sin k\tau), \tag{11}$$

where the coefficients $\mathbf{c}_k, \mathbf{s}_k$ are vectors of dimension 2×1. Equation 11, usually referred to as the rule of solution expression, can guide us in choosing the following linear operator and initial guess of the solution.

Let $a_0, h_0, \omega_0, \beta_0$ and $\mathbf{x}_0(\tau)$ denote the initial approximations of a, h, ω, β and $\mathbf{x}(\tau)$, respectively. According to the rule of solution expression and the initial conditions, an initial guess of the solution can be given as:

$$\mathbf{x}_0(\tau) = \begin{bmatrix} h_0 \cos\tau + \beta_0 \sin\tau & a_0 \cos\tau \end{bmatrix}^T. \tag{12}$$

3.2. Zeroth-order deformation equation

The homotopy analysis method is based on the continuous variations $A(p)$, $H(p)$, $\Omega(p)$, $B(p)$ and $\mathbf{u}(\tau, p)$. As the embedding parameter p increases from 0 to 1, $\mathbf{u}(\tau, p)$ varies from the initial guess $\mathbf{x}_0(\tau)$ to the exact solution, and at the same time $A(p)$, $H(p)$, $\Omega(p)$, $B(p)$ vary from the initial approximations a_0, h_0, ω_0, β_0 to a, h, ω, β, respectively.

Due to the rule of solution expression, one may define the linear auxiliary operator as

$$L[\mathbf{u}(\tau, p)] = \omega_0^2 \left[\frac{\partial^2 \mathbf{u}(\tau, p)}{\partial \tau^2} + \mathbf{u}(\tau, p) \right], \tag{13}$$

thus

$$L\left[\begin{pmatrix} \cos\tau \\ \sin\tau \end{pmatrix} \right] = \mathbf{0}. \tag{14}$$

According to equation 9, the nonlinear operator should be chosen as

$$\begin{aligned} N[\mathbf{u}(\tau, p), \Omega(p)] &= \Omega^2(p)\mathbf{M}\frac{\partial^2 \mathbf{u}(\tau, p)}{\partial \tau^2} + \Omega(p)\boldsymbol{\mu}\frac{\partial \mathbf{u}(\tau, p)}{\partial \tau} \\ &+ \mathbf{K}\mathbf{u}(\tau, p) + \mathbf{C}\mathbf{W}(\mathbf{u}(\tau, p), \Omega(p)) + \mathbf{F}(\mathbf{u}(\tau, p)). \end{aligned} \tag{15}$$

Then, based on the homotopy analysis method, a family of equations can be constructed,

$$(1 - p)L[\mathbf{u}(\tau, p) - \mathbf{x}_0(\tau)] = \lambda\, pN[\mathbf{u}(\tau, p), \Omega(p)], \tag{16}$$

subject to the initial conditions

$$\mathbf{u}(0, p) = \begin{bmatrix} H(p) & A(p) \end{bmatrix}^T, \quad \left.\frac{\partial \mathbf{u}(\tau, p)}{\partial \tau}\right|_{\tau=0} = \begin{bmatrix} B(p) & 0 \end{bmatrix}^T, \tag{17}$$

where the auxiliary parameter λ is a non-zero constant. Equation 16 is usually called the zeroth-order deformation equation.

3.3. High-order deformation equations

When $p = 0$, equations 16 and 17 have the solution

$$\mathbf{u}(\tau,\ 0) = \mathbf{x}_0(\tau); \tag{18}$$

when $p = 1$, they are exactly the same as equations 9 and 10 provided that

$$\mathbf{u}(\tau,\ 1) = \mathbf{x}(\tau), \quad A(1) = a, \quad H(1) = h, \quad \Omega(1) = \omega, \quad B(1) = \beta. \tag{19}$$

Expand $A(p)$, $H(p)$, $\Omega(p)$, $B(p)$ and $\mathbf{u}(\tau, p)$ as series in p:

$$\begin{aligned} \mathbf{u}(\tau, p) &= \sum_{k=0}^{\infty} \mathbf{u}_k(\tau) p^k, \quad A(p) = \sum_{k=0}^{\infty} a_k p^k, \quad H(p) = \sum_{k=0}^{\infty} h_k p^k, \\ \Omega(p) &= \sum_{k=0}^{\infty} \omega_k p^k, \quad B(p) = \sum_{k=0}^{\infty} \beta_k p^k. \end{aligned} \tag{20}$$

As long as the parameter λ is appropriately chosen, all of these series are convergent at $p = 1$. Then, the nth-order homotopy analysis approximations can be given as

$$\mathbf{x}(\tau) = \sum_{k=0}^{n} \mathbf{u}_k(\tau), \quad a = \sum_{k=0}^{n} a_k, \quad h = \sum_{k=0}^{n} h_k, \quad \omega = \sum_{k=0}^{n} \omega_k, \quad \beta = \sum_{k=0}^{n} \beta_k. \tag{21}$$

Substituting equation 20 into equations 16 and 17 and then equating the coefficients of p^k to zero results in the kth-order deformation equation

$$L[\mathbf{u}_k(\tau) - \chi_k \mathbf{u}_{k-1}(\tau)] = \lambda \, \mathbf{R}_k(\tau), \tag{22}$$

subject to the initial conditions

$$\mathbf{u}_k(0) = \begin{bmatrix} h_k & a_k \end{bmatrix}^T, \quad \mathbf{u}_k'(0) = \begin{bmatrix} \beta_k & 0 \end{bmatrix}^T, \tag{23}$$

where

$$\mathbf{R}_k(\tau) = \frac{1}{(k-1)!} \left. \frac{\partial^{k-1} N[\mathbf{u}(\tau, p), \Omega(p)]}{\partial p^{k-1}} \right|_{p=0} \tag{24}$$

and

$$\chi_k = \begin{cases} 0, & k = 1, \\ 1, & k \geq 2. \end{cases} \tag{25}$$

Due to the rule of solution expression and the linear operator L, the right-hand side of equation 22 should not contain $\sin\tau$ and $\cos\tau$, because they can respectively result in such so-called secular terms as $\tau \sin\tau$ and $\tau \cos\tau$. Thus, one can determine a_0, h_0, ω_0 and β_0 by solving

$$\begin{aligned} \mathbf{\Gamma}^c_{1,1}(a_0, h_0, \omega_0, \beta_0) &= \frac{1}{\pi} \int_0^{2\pi} \mathbf{R}_1(\tau) \cos\tau \, d\tau = 0, \\ \mathbf{\Gamma}^s_{1,1}(a_0, h_0, \omega_0, \beta_0) &= \frac{1}{\pi} \int_0^{2\pi} \mathbf{R}_1(\tau) \sin\tau \, d\tau = 0. \end{aligned} \tag{26}$$

One can see that the zeroth-order homotopy analysis approximation is independent of λ. In fact, equation 26 can also be deduced by the harmonic balance method.

After obtaining a_0, h_0, ω_0 and β_0, $\mathbf{x}_0$ (that is, $\mathbf{u}_0$) can then be uniquely determined. Substituting a_0, h_0, ω_0, β_0 and $\mathbf{u}_0$ into equation 22 yields $\mathbf{u}_1(\tau)$. Observe that $\mathbf{u}_1(\tau)$ is linear with respect to h_1, a_1 and β_1. Likewise, $\mathbf{u}_k$ depends linearly on a_k, h_k and β_k when $k > 1$.

If $a_{k-1}, h_{k-1}, \omega_{k-1}, \beta_{k-1}$ and $\mathbf{u}_{k-1}(\tau)$ are all known, the kth-order approximations are governed by the following linear algebraic equations

$$\begin{aligned}\boldsymbol{\Gamma}^c_{k+1,1}(a_k, h_k, \omega_k, \beta_k) &= \frac{1}{\pi}\int_0^{2\pi} \mathbf{R}_{k+1}(\tau)\cos\tau d\tau = 0,\\ \boldsymbol{\Gamma}^s_{k+1,1}(a_k, h_k, \omega_k, \beta_k) &= \frac{1}{\pi}\int_0^{2\pi} \mathbf{R}_{k+1}(\tau)\sin\tau d\tau = 0,\end{aligned} \tag{27}$$

where $k \geq 1$. In order to show that equations 27 are linear as $k \geq 1$, we consider the relationship between $\mathbf{R}_{k+1}(\tau)$ and $a_k, h_k, \omega_k, \beta_k$. Firstly, $\mathbf{R}_{k+1}(\tau)$ is rewritten as

$$\begin{aligned}\mathbf{R}_{k+1}(\tau) &= \mathbf{M}\sum_{i=0}^{k}\sum_{j=i}^{k}\omega_i\omega_{j-i}\mathbf{u}''_{k-j} + \boldsymbol{\mu}\sum_{i=0}^{k}\omega_i\mathbf{u}'_{k-i} + \mathbf{K}\mathbf{u}_k\\ &+ \mathbf{C}\sum_{i=0}^{k}\left.\frac{\partial^{k-i}\mathbf{W}\left(\mathbf{u}_i, \sum_{j=0}^{k-i}\omega_j p^j\right)}{\partial\, p^{k-i}}\right|_{p=0}\\ &+ \left[\begin{array}{cc} c_{10}\gamma\sum_{i=0}^{k}\sum_{j=i}^{k}\mathbf{u}_i^{(1)}\mathbf{u}_{j-i}^{(1)}\mathbf{u}_{k-j}^{(1)} & d_{10}\eta\sum_{i=0}^{k}\sum_{j=i}^{k}\mathbf{u}_i^{(2)}\mathbf{u}_{j-i}^{(2)}\mathbf{u}_{k-j}^{(2)}\end{array}\right]^T\\ &= \mathbf{N_1}u_k + \mathbf{N_2}\omega_k,\end{aligned} \tag{28}$$

where $\mathbf{u}_i^{(1)}$ and $\mathbf{u}_i^{(2)}$ denote the first and second component of $\mathbf{u}_i$, respectively. Vectors $\mathbf{N_1}$, $\mathbf{N_2}$ are functions of $a_0, h_0, \beta_0, \omega_0, \cdots, a_{k-1}, h_{k-1}, \beta_{k-1}, \omega_{k-1}$ and τ, but independent of $a_k, h_{k,}\omega_k$ and β_k. In addition, as mentioned above, $\mathbf{u}_k(\tau)$ is linear with respect to h_k, a_k and β_k, thus $\mathbf{R}_{k+1}(\tau)$ must be linearly related to a_k, h_k, ω_k and β_k. Accordingly, equations 27 are linear when $k \geq 1$, which implies that it is rather easy to obtain the high-order approximations.

4. NUMERICAL EXAMPLES

The system parameters under consideration are $\mu = 100$, $r_\alpha = 0.5$, $a_h = -0.5$, $\zeta_\alpha = \zeta_\xi = 0$, $\bar{\omega} = 0.25$, $x_\alpha = 0.25$, $\gamma = 0$, and $\eta = 80$. Numerical solutions are obtained by numerically integrating equation 4 subject to the initial conditions as $\alpha(0) = 1^\circ$ and $\dot{\alpha}(0) = \xi(0) = \dot{\xi}(0) = 0$. In addition, after obtaining the homotopy analysis approximation

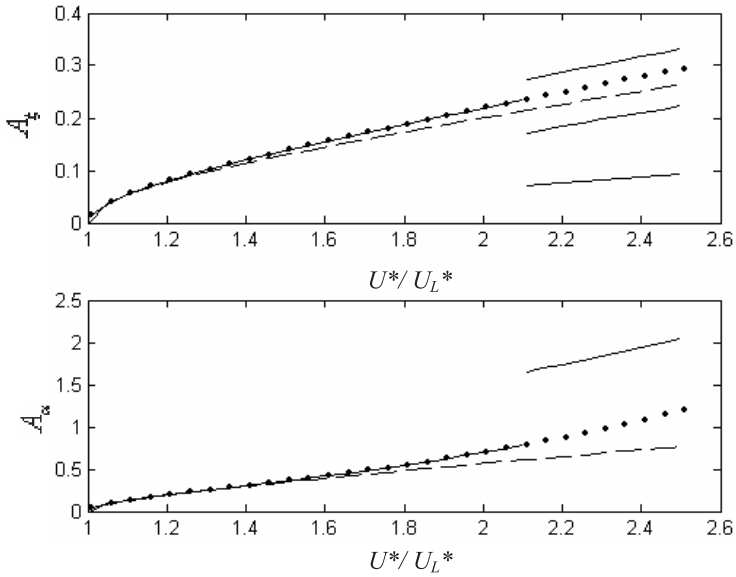

Figure 2. Comparisons of the homotopy analysis approximations for the amplitudes with the harmonic balance results and numerical solutions: 30th-order homotopy analysis approximations when $\lambda = -1$ (dotted lines); harmonic balance results; and real lines: numerical solutions (dashed lines).

x, the amplitudes of the limit cycle oscillation in the plunge and pitch motions can be defined as A_ξ and A_α, corresponding to the extremes of $\xi(t)$ and $\alpha(t)$, respectively.

By using analytical techniques developed for nonlinear dynamical systems, the linear flutter speed is found to be $U^* = U_L^* = 6.0385$. As U^* increases through U_L^*, the equivalent point loses is its stability and limit cycle oscillation arises, hence U_L^* is a Hopf bifurcation point. There is a secondary Hopf bifurcation as U^* increases further, where a jump of the amplitudes is detected. Liu and Dowell (2004) also found that in order to predict the secondary bifurcation, at least nine (or five dominant) harmonics must be taken into account when using the high-dimensional harmonic balance method.

The zeroth-order homtopy analysis approximation is essentially the same as that attained by the harmonic balance method, namely the harmonic balance solution. The high-order approximations are obtained based on those of zeroth order. Consequently, the proposed approach is not capable of predicting the second bifurcation. Nevertheless, validity and high efficiency can still be observed from Figures 2 and 3. The two figures show the 30th-order homotopy analysis approximations, the harmonic balance as well as the numerical solutions of the amplitudes and frequencies of the limit cycle oscillations. The homotopy analysis approximations are almost the same as the numerical ones, but the errors in the harmonic balance results increase with U^*.

The phase planes of the limit cycle oscillation of the airfoil when $U^* = 1.5U_L^*$ and $U^* = 2U_L^*$ are plotted in Figures 4 and 5, respectively. Excellent agreement of the homotopy analysis approximations with numerical solutions is evident. Although the harmonic balance

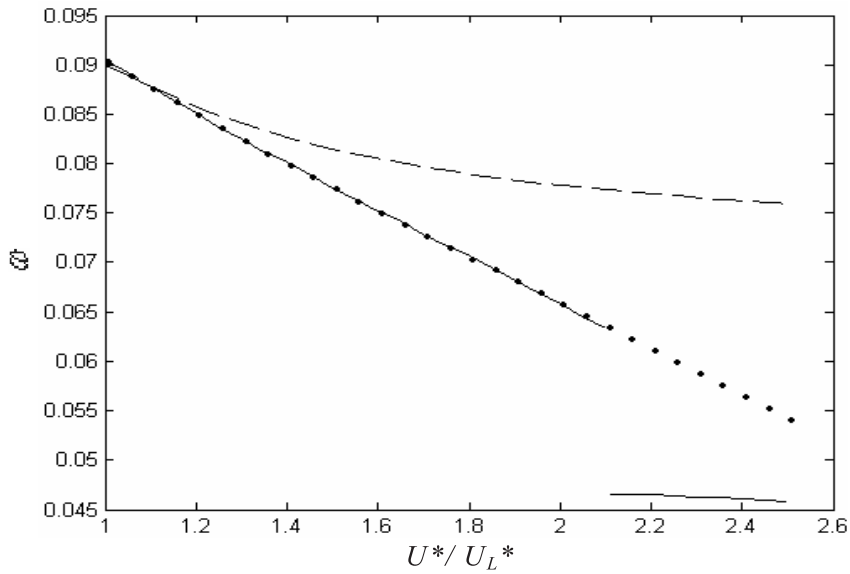

Figure 3. Comparisons of the homotopy analysis approximation for the frequency with the harmonic balance result and numerical solution: 30th-order homotopy analysis approximations when $\lambda = -1$ (dotted line); harmonic balance results (dashed line); and numerical solutions (solid line).

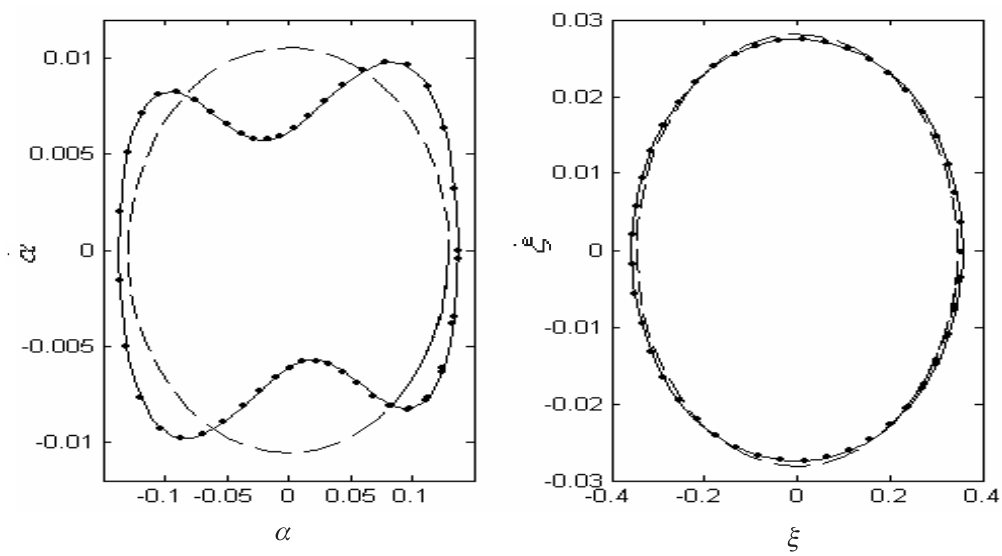

Figure 4. Phase planes of the limit cycle oscillation when $U^* = 1.5\ U_L^*$: 20th-order homotopy analysis approximations when $\lambda = -1$ (dotted curves); harmonic balance results (dashed curves); numerical solutions (solid curves).

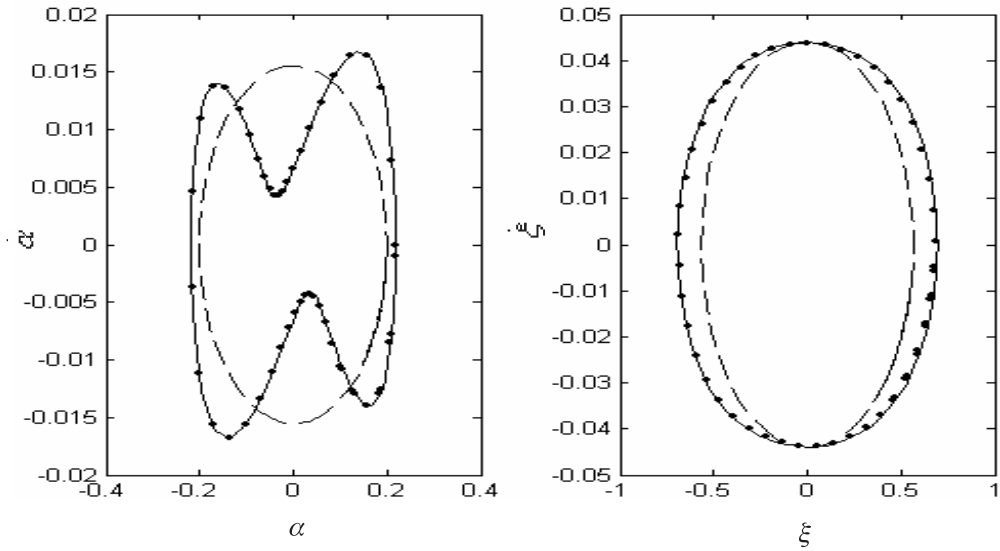

Figure 5. Phase planes of the limit cycle oscillation when $U^* = 2\ U_L^*$: 20th-order homotopy analysis approximations when $\lambda = -1$ (dotted curves); harmonic balance results (dashed curves); numerical solutions (solid curves).

solution of the plunge motions is also very accurate when $U^* = 1.5U_L^*$, the discrepancy becomes very large when $U^* = 2U_L^*$.

The convergence of equations 20 depends upon the auxiliary parameter λ. Figure 6 plots the curves of the relative errors of the homotopy analysis approximations versus λ. In the convergent region, say $\lambda \in (-1.4, 0)$, the smaller λ is chosen, the more accurate the approximation is. The radius of convergence of equations 20 can be determined as $r_\omega = \lim_{k\to\infty} \omega_k^{-1/k}$ by the root criterion for series convergence. Figure 7 shows that when λ is in the convergent region, the radius enlarges as λ decreases. But the radius becomes less than 1 if λ is beyond the convergent region (for example, $\lambda = -1.5$), which may result in the divergence of equations 20 at $p = 1$.

For the choice of the auxiliary parameter λ, two issues should be considered: whether equations 20 converge and the rate of convergent. According to the above discussion, on the one hand, we need to choose the auxiliary parameter as small as possible to improve the convergent rate. But on the other hand, we are prone to choose an improper value, causing equations 20 to diverge at $p = 1$.

As is shown in Figure 8b, most of the computational effort spent in seeking $\mathbf{u}_k$ is taken up with the Fourier series expansion of $\mathbf{x}^3$, especially when k is relatively large. If the transformation $\mathbf{x} = \mathbf{\Lambda y}$ is applied to equation 7, $\mathbf{x}^3$ will become $\mathbf{\Lambda}^3\mathbf{y}^3$. More and more time is spent on expanding $\mathbf{\Lambda}^3\mathbf{y}^3$ than $\mathbf{x}^3$, as shown in part (a) of Figure 8. Therefore, it is computationally advantageous to abandon the transformation $\mathbf{x} = \mathbf{\Lambda y}$.

We now turn to discuss the relationship between the convergence of equations 20 and the coefficient of the cubic nonlinearity, η. Interestingly, it is found that ω_i is independent of η, and that a_i, β_i and h_i are inversely proportional to $\sqrt{\eta}$. Thus, the convergence of

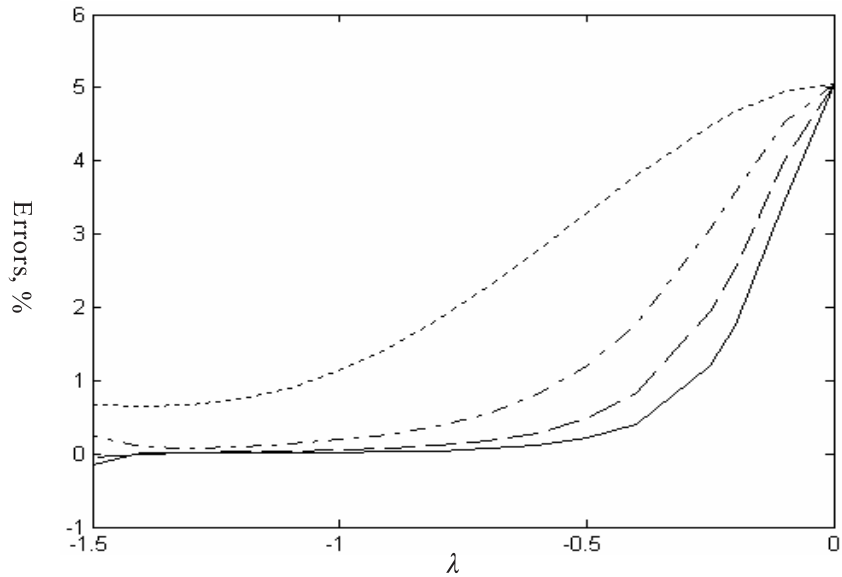

Figure 6. Relative errors of the homotopy analysis approximations for the frequency when $U^* = 1.5U_L^*$ versus λ: 5th-order approximations (dotted line); 10th-order approximations (dash-dotted line); 15th-order approximations (dashed line); 20th-order approximations (solid line).

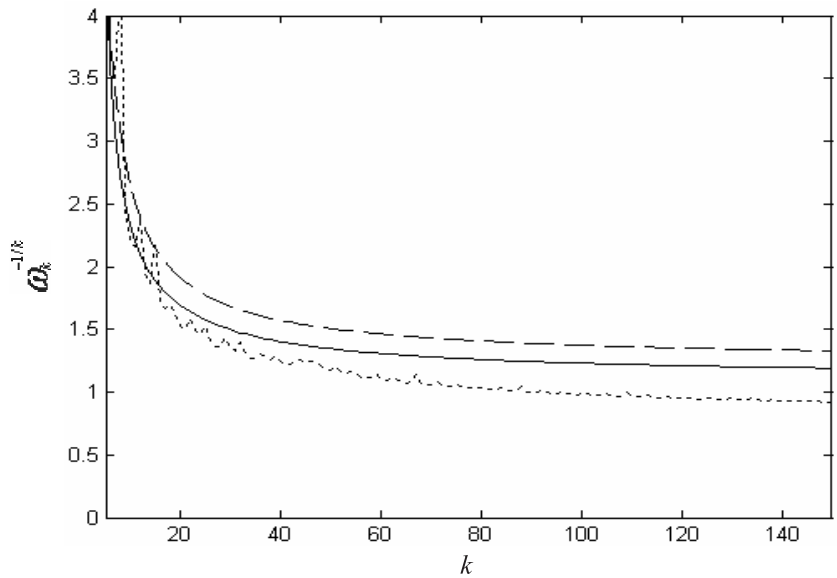

Figure 7. Root criterion for series convergence for the series expansion for the frequency when $U^* = 1.5U_L^*$: $\lambda = -0.5$ (solid line); $\lambda = -1$ (dashed line); $\lambda = -1.5$ (dotted line).

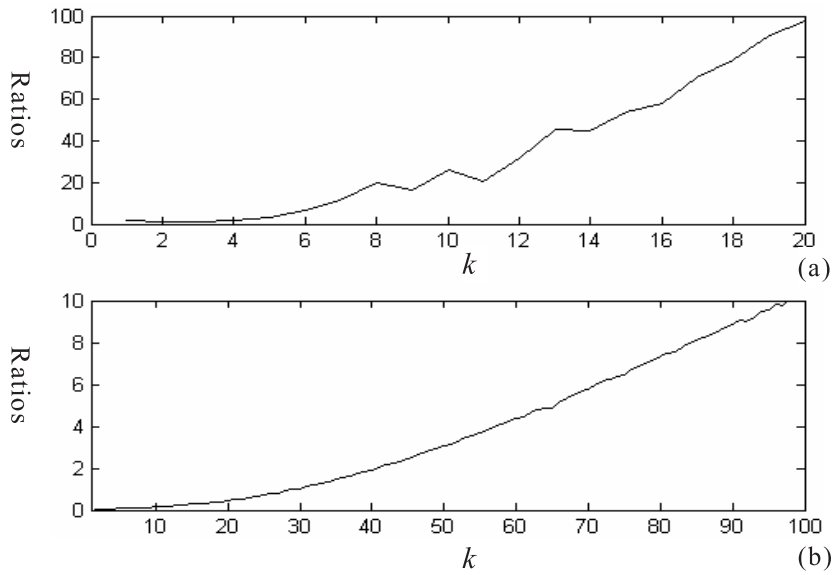

Figure 8. Ratios of the time spent expanding $\mathbf{x}^3$: (a) to give $\mathbf{\Lambda}^3\mathbf{y}^3$ when obtaining $\mathbf{u}_k$; (b) to the total time for obtaining $\mathbf{u}_k$.

equations 20 is independent of η and hence the proposed method is valid for both weakly and strongly nonlinear problems. Furthermore, it turns out that the frequency of the limit cycle oscillation of the considered aeroelastic system is independent of η, while the amplitudes are inversely proportional to $\sqrt{\eta}$. If $A_\alpha(\eta)$ and $A_\xi(\eta)$ are introduced to represent the amplitudes of the limit cycle oscillation of pitch and plunge motions as functions of η, they are given by $A_\alpha(\eta) = A_\alpha(1)/\sqrt{\eta}$ and $A_\xi(\eta) = A_\xi(1)/\sqrt{\eta}$. The amplitudes of the limit cycle oscillations versus η when $U_L = 1.5U_L^*$ are shown in Figure 9, where $A_\alpha(1)$ and $A_\xi(1)$ are given by the 20th-order homotopy analysis approximations when $\eta = 1$. Both the homotopy analysis approximations and numerical solutions are in excellent agreement with the curves given by $A_\alpha(\eta) = A_\alpha(1)/\sqrt{\eta}$ and $A_\xi(\eta) = A_\xi(1)/\sqrt{\eta}$.

Interestingly, the relationships still exist when U^* is larger than the value at which the secondary Hopf bifurcation occurs. Figure 10 shows the curves of the amplitudes versus η when $U^* = 2.5\ U_L^*$, where $A_\alpha(1)$ and $A_\xi(1)$ are obtained by numerically integrating equation 4 when $\eta = 1$.

5. CONCLUSIONS AND REMARKS

We have employed the homotopy analysis method to propose an analytical approach for nonlinear aeroelastic systems. The frequencies and amplitudes of the limit cycle oscillations can be obtained to any desired accuracy. Importantly, highly accurate solutions are obtained just by solving linear equations. A major finding of this study is the relationships between the amplitudes (or frequencies) of limit cycle oscillations and the coefficient of the cubic

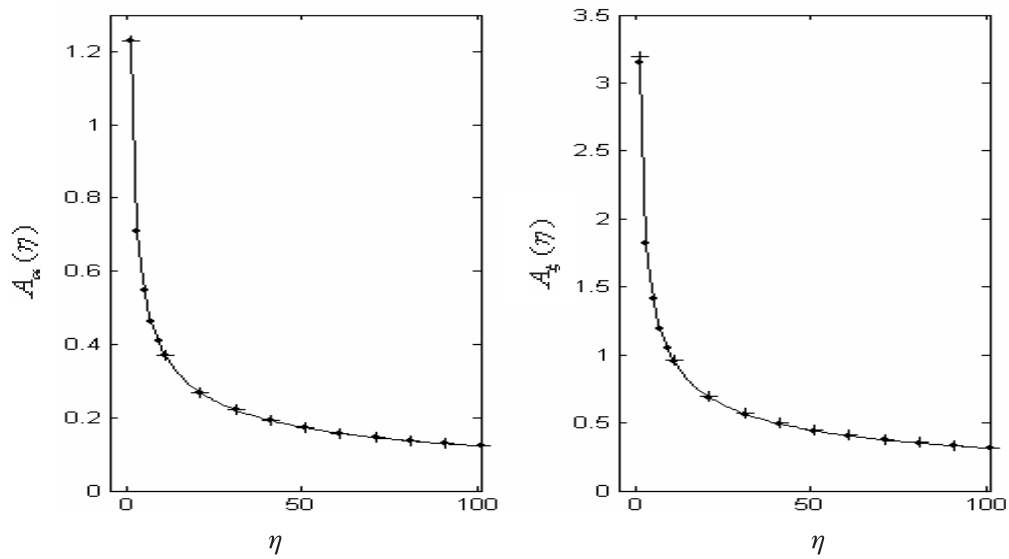

Figure 9. Curves of the amplitudes of limit cycle oscillations when $U^* = 1.5\ U_L^*$ versus η: $A_\alpha(\eta) = A_\alpha(1)/\sqrt{\eta}$ and $A_\xi(\eta) = A_\xi(1)/\sqrt{\eta}$ (solid lines); 20th-order homotopy analysis approximations when $\lambda = -1$ (dots); numerical solutions (+).

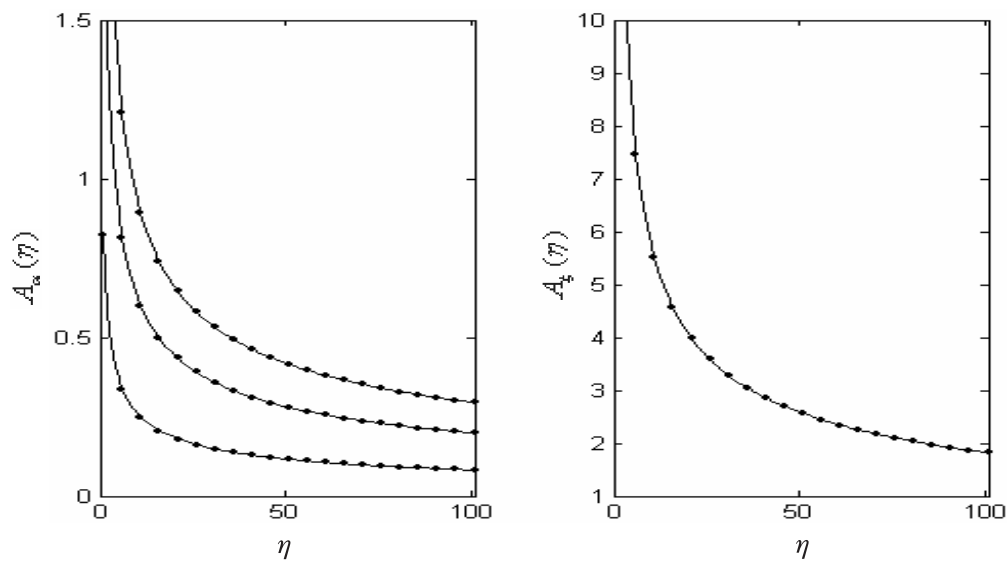

Figure 10. Curves of the amplitudes of limit cycle oscillations when $U = 2.5\ U_L^*$ versus η: $A_\alpha(\eta) = A_\alpha(1)/\sqrt{\eta}$ and $A_\xi(\eta) = A_\xi(1)/\sqrt{\eta}$ (solid lines); numerical solutions (dots).

nonlinearity. The approach presented is very effective for both weakly and strongly nonlinear aeroelastic systems, which implies that we can expect this approach to be applicable to other nonlinear dynamic systems, especially those containing strong nonlinearites.

APPENDIX: EXPRESSIONS FOR THE COEFFICIENTS IN EQUATION 3

$$
\begin{aligned}
c_0 &= 1+\frac{1}{\mu}, \quad c_1 = x_\alpha - \frac{a_h}{\mu}, \quad c_2 = \frac{2}{\mu}(1-\psi_1-\psi_2) + 2\zeta_\xi \frac{\overline{\omega}}{U^*},\\
c_3 &= \frac{1}{\mu}(1+(1-2a_h)(1-\psi_1-\psi_2)), \quad c_4 = \frac{2}{\mu}(\varepsilon_1\psi_1+\varepsilon_2\psi_2),\\
c_5 &= \frac{2}{\mu}\left(1-\psi_1-\psi_2+\left(\frac{1}{2}-a_h\right)(\varepsilon_1\psi_1+\varepsilon_2\psi_2)\right),\\
c_6 &= \frac{2}{\mu}\varepsilon_1\psi_1\left(1-\varepsilon_1\left(\frac{1}{2}-a_h\right)\right), \quad c_7 = \frac{2}{\mu}\varepsilon_2\psi_2\left(1-\varepsilon_2\left(\frac{1}{2}-a_h\right)\right),\\
c_8 &= -\frac{2}{\mu}\varepsilon_1^2\psi_1, \quad c_9 = -\frac{2}{\mu}\varepsilon_2^2\psi_2, \quad c_{10} = \left(\frac{\overline{\omega}}{U^*}\right)^2,\\
d_0 &= \frac{x_\alpha}{r_\alpha^2} - \frac{a_h}{\mu\, r_\alpha^2}, \quad d_1 = 1+\frac{1+8a_h^2}{8\mu\, r_\alpha^2}, \quad d_2 = -\frac{1+2a_h}{\mu\, r_\alpha^2}(\varepsilon_1\psi_1+\varepsilon_2\psi_2),\\
d_3 &= \frac{1-2a_h}{2\mu\, r_\alpha^2} - \frac{(1-4a_h^2)(1-\psi_1-\psi_2)}{2\mu\, r_\alpha^2} + \frac{2\zeta_\alpha}{U^*}, \quad d_4 = -\frac{1+2a_h}{\mu\, r_\alpha^2}(\varepsilon_1\psi_1+\varepsilon_2\psi_2),\\
d_5 &= -\frac{1+2a_h}{\mu\, r_\alpha^2}(1-\psi_1-\psi_2) - \frac{(1+2a_h)(1-2a_h)(\psi_1\varepsilon_1-\psi_2\varepsilon_2)}{2\mu\, r_\alpha^2},\\
d_6 &= -\frac{(1+2a_h)\psi_1\varepsilon_1}{\mu\, r_\alpha^2}\left(1-\varepsilon_1\left(\frac{1}{2}-a_h\right)\right),\\
d_7 &= -\frac{(1+2a_h)\psi_2\varepsilon_2}{\mu\, r_\alpha^2}\left(1-\varepsilon_2\left(\frac{1}{2}-a_h\right)\right), \quad d_8 = \frac{(1+2a_h)\psi_1\varepsilon_1^2}{\mu r_\alpha^2},\\
d_9 &= \frac{(1+2a_h)\psi_2\varepsilon_2^2}{\mu\, r_\alpha^2}, \quad d_{10} = \left(\frac{1}{U^*}\right)^2.
\end{aligned}
$$

Acknowledgments. This work is supported by the NSFC (10772202), the Doctoral Program Foundation of the Ministry of Education of China (20050558032), and the Guangdong Province Natural Science Foundation (07003680, 05003295).

REFERENCES

Alexander, J. C. and Yorke, J. A., 1978, "The homotopy continuation method: Numerically implementable topological procedures," *Transactions of the American Mathematical Society* **242**, 271–284.

El-Wakil, S. A. and Abdou, M. A., 2008, "New applications of the homotopy analysis method," *Zeitschrift für Naturforschung A* **63**, 385–392.

Jones, R. T., 1940, *The Unsteady Lift of a Wing of Finite Aspect Ratio*, NACA Report 681.

Lee, B. H. K., Gong, L., and Wong, Y. S., 1997, "Analysis and computation of nonlinear dynamic response of a two-degree-of-freedom system and its application in aeroelasticity," *Journal of Fluids and Structures* **11**, 225–246.

Lee, B. H. K., Liu, L., and Chung, K. W., 2005, "Airfoil motion in subsonic flow with strong cubic nonlinear restoring forces," *Journal of Sound and Vibration* **281**, 699–717.

Lee, B. H. K., Price, S. J., and Wong, Y. S., 1999, "Nonlinear aeroelastic analysis of airfoils: bifurcation and chaos," *Progress in Aerospace Science* **35**, 205–344.

Liao, S. J., 2003, *Beyond Perturbation: Introduction to Homotopy Analysis Method*, Chapman & Hall/CRC Press, Boca Raton, FL.

Liao, S. J., 2004, "An analytic approximate approach for free oscillations of self-excited system," *International Journal of Non-Linear Mechanics* **39**, 271–280.

Liu, J. K. and Zhao, L. C., 1992, "Bifurcation analysis of airfoils in incompressible flow," *Journal of Sound and Vibration* **154(1)**, 117–124.

Liu, L., Wong, Y. S., and Lee, B. H. K., 2000, "Application of the center manifold theory in nonlinear aeroelasticity," *Journal of Sound and Vibration* **234**, 641–659.

Liu, L. P. and Dowell, E. H., 2004, "The secondary bifurcation of an aeroelastic airfoil motion: Effect of high harmonics," *Nonlinear Dynamics* **37**, 31–49.

Liu, L. P., Dowell, E. H., and Thomas, J. P., 2007, "A high dimensional harmonic balance approach for an aeroelastic airfoil with cubic restoring forces," *Journal of Fluids and Structures* **23**, 351–363.

Nayfeh, A. H., 1981, *Introduction to Perturbation Techniques*, Wiley, New York.

Price, S. J., Alighanbari, H., and Lee, B. H. K., 1995, "The aeroelastic response of a two-dimensional airfoil with bilinear and cubic structural nonlinearities," *Journal of Fluids and Structures* **9**, 175–193.

Raghothama, A. and Narayanan, S., 1999, "Nonlinear dynamics of a two-dimensional airfoil by incremental harmonic balance method," *Journal of Sound and Vibration* **226(3)**, 493–517.

Shahrzad, P. and Mahzoon, M., 2002, "Limit cycle flutter of airfoils in steady and unsteady flows," *Journal of Sound Vibration* **256(2)**, 213–225.

Ueda, T. and Dowell, E. H., 1984, "Flutter analysis using nonlinear aerodynamic forces," *Journal of Aircraft* **21**, 101–109.